Available online at www.sciencedirect.com
SCIENCE DIRECT®
Journal of Molecular Catalysis A: Chemical 236 (2005) 77–86
JOURNAL OF MOLECULAR CATALYSIS A: CHEMICAL
www.elsevier.com/locate/molcata

Investigations on gold nanoparticles in mesoporous and microporous materials

Deepak B Akolekar *, Suresh K Bhargava **

Catalysis and Advanced Materials Research Group School of Applied Sciences, Science, Engineering and Technology Portfolio, RMIT University, City Campus, Melbourne, Victoria 3001, Australia

Received 14 February 2005; received in revised form 30 March 2005; accepted 31 March 2005
Available online 23 May 2005

Abstract

The gold nanoparticles in different high surface area mesoporous and microporous materials were prepared using sol–gel and hydrothermal crystallization methods. For investigating the characteristics behaviour of nano gold particles in the mesoporous and microporous materials, Au-Al-MCM-41, Au-ZSM-5 and Au-LSX were prepared with different framework composition and concentrations of gold nanoparticles. The Au-Al-MCM-41, Au-ZSM-5 and Au-LSX samples were characterized using the BET, FTIR, ICP-MS, XAS, XPS, TEM and XRD. The XPS measurements indicate that the presence of gold species in different oxidation state and concentration of gold metal species varies over the surfaces of as-synthesized and calcined gold containing mesoporous and microporous materials.

In these materials, the size of gold nanoparticles varied in the range of ~2–6 nm. The dispersion and size of gold nanoparticles are different in the materials with MCM-41, ZSM-5 and LSX structures. The interaction of NO/CO with the nano gold materials under different reaction temperatures and NO/CO pressures have been studied using in-FTIR technique. In situ high temperature XRD measurements were conducted over the materials in order to investigate the fate of gold nanoparticles and phase transformations at high temperatures (303–1873 K) within the mesoporous and microporous matrices.

Keywords: Gold nanoparticles; Mesoporous materials; MCM-41; Microporous materials; ZSM-5; LSX; Low silica faujasite; Surface properties; Au; XRD; Synthesis. In situ HTXRD

1. Introduction

Currently nano-materials attract considerable attention due to a variety of novel features. New physical, chemical, and thermodynamic properties are expected to occur in such systems, arising from the large fraction of low coordinated atoms at the surface and the confinement of electrons to a rather small volume, respectively [1]. From a technical point of view, however, the development of future applications will need to adhere/support the nanoscaled materials on suitable substrates in two- or three-dimensional arrangements in order to take advantage of their fascinating properties under different conditions.

Gold exhibits a unique catalytic nature and action when it is deposited as nanoparticles on a variety of metal oxides. Currently, nano gold materials are employed in low temperature CO oxidation in hydrogen stream, CO gas sensors, selective oxidation of alkanes, olefins, and alcoholic compounds, oxidation of nitrogen-containing compounds, selective hydrogenation of 1,3-butadiene, methanol synthesis, reduction of NO_x, etc. [2–9]. The catalytic and adsorption properties are influenced by the dispersion, structure and interaction of gold nanoparticles with the support as well as by the support type [8,10–13].

The new generation microporous and mesoporous materials are increasingly being used in various commercial catalysts because of their high surface area, unique pore sizes,

* Corresponding author. Tel.: +61 3 99252121; fax: +61 2 96391321.
** Corresponding author.
E-mail addresses: E04781@ems.rmit.edu.au (D.B. Akolekar), suresh.bhargava@rmit.edu.au (S.K. Bhargava).

1381-1169/$ – see front matter © 2005 Elsevier B.V. All rights reserved.
doi:10.1016/j.molcata.2005.03.048

thermal stability, etc. Materials such as ZSM-5 and MCM-41 are suitably employed as catalyst/ support/adsorbents. MCM-41 and ZSM-5 are high surface area materials with regular, well-defined pore systems, low acidity and thermal stability. For enhancing catalytic activities, these material properties could be easily manipulated by inclusion of active nano metal particles/other elements into the framework. The catalytic properties of these materials largely depend upon the Si/Al ratio, degree of cation exchange, extra-/framework element, surface treatment etc [14–18]. The major problem faced by the gold nanoparticles in the high temperature catalysis/other applications is the particle aggregation/sintering/clustering, thus affecting the catalytic performance and restricting their usage at high temperatures.

The main aims of this study were to prepare and characterize gold nanoparticles containing mesoporous and microporous materials, determine the interactions towards the air pollutants and to investigate the influence of high temperatures on the gold nanoparticles within microporous and mesoporous structures. So far, the in situ FTIR NO/CO and in situ high XRD temperature studies reported on gold nanoparticles within mesoporous and microporous catalytic materials are limited. The gold catalysts prepared by different methods and using different supports (MCM-41, ZSM-5, LSX) were investigated. The advantage of using microporous and mesoporous materials for gold nanoparticles inclusion is that the metal particle size can be contained at certain levels during catalytic treatments and usage at higher temperatures.

2. Experimental section

The mesoporous (MCM-41) and microporous (ZSM-5, X) materials containing gold nanoparticles were prepared using well-known hydrothermal crystallization methods [19–23]. The mesoporous (MCM-41) and microporous (ZSM-5) materials containing gold particles were prepared with different Si/Al ratios and gold concentrations.

The Au-Al-MCM-41 catalysts were prepared by hydrothermal synthesis of a mixture consisting of dilute gold salt solution, Ludox AS-40 (40 wt.% silica in water stabilized with ammonia), sodium aluminate solution, tetraethylammonium hydroxide (20 wt.%), cetyltrimethylamonium bromide (CTAB) and water. The synthetic mixture was prepared by mixing appropriate amount of Ludox, metal salt solution, sodium aluminate solution, tetraethylammonium hydroxide and CTAB for 3.6 h at room temperature. In the preparation of Au-Al-MCM-41(a), the initial Si/Al and Si/Au ratios were 27 and 35 while in the Au-Al-MCM-41(b), the initial Si/Al and Si/metal ratios were 27 and 230, respectively. After stirring was complete, the mixture was transferred to an Teflon coated autoclave and heated at 368 K for 75 h. During synthesis, pH was maintained between 11.0 and 12.1 was using acid. The mesoporous material was thoroughly washed with de-ionised water, dried at 340 K for 29 h and calcined at 773 K for 18 h.

The Au-ZSM-5 catalysts were prepared by hydrothermal synthesis of a gel consisting of active sources of gold, silicon, aluminium, and template. The synthetic gel mixture (with the Si/Al ratios 36, 44, 61 and Si/Au ratios 510, 89, 76) was prepared by mixing appropriate amount of fumed silica, metal salt solution, aluminium chloride solution, tetrapropylammonium hydroxide (20 wt.%) for 4.0 h at room temperature. After stirring was complete, the mixture was transferred to an Teflon coated autoclave and heated at 433 K for 120 h. The material was thoroughly washed with de-ionised water, dried at 340 K for 29 h and calcined at 763 K for 18 h. The Au-LSX was prepared according to the method reported elsewhere [22] along with the addition of appropriate amount of dilute gold compound solution during the gel preparation. The Au-LSX was synthesized at 348 K for 144 h. The chemicals used in synthesis of these materials were Catapal (aluminium oxyhydroxide), Aerosil (fumed silica), Ludox HS-40 (Aldrich), tetrapropylammonium hydroxide (Aldrich), cetyl tri-methyl ammonium chloride (CTACl) solution (Aldrich), sodium hydroxide (BDH), and water based gold chloride solution.

For studying the influence of high temperatures on the properties of gold nanoparticles, the as-prepared Au-Al-MCM-41(a) sample was heated at different temperatures (823, 1123 and 1273 K) in an inert (helium) atmosphere.

The standard and sophisticated instrumental techniques such as ICP-MS (HP4500 Series 300), XRD (Bruker D8 Advance), BET, TEM (JEOL 2010), XAS [12] were used to characterize the materials for their chemical composition, phase purity, structure, surface properties and particle size etc., respectively. For the ICPMS analysis, the samples were completely dissolved by acid digestion (hydrofluoric, a mixture of hydrochloric and nitric acids). The surface area and micro- and total-pore volume of the materials were obtained by N_2-dynamic adsorption/desorption technique ($p/p_o = 0.3$) using a Micromeritics ASAP2000 Instrument. Powder X-ray diffraction patterns were obtained with a Bruker D8 Advance XRD (using a Ni-α filtered Cu Kα X-ray source) and in situ high temperature attachments (HTK2000). In situ high temperature XRD experiments were conducted under vacuum. XPS analysis was conducted for determining the surface concentration and binding energy using a Fisons system (operated in the constant pass energy mode of 20 eV). An Mg Kα X-ray source ($h\nu = 1253.7$ eV) was operated at 20 mA and 15 mV. The base pressure of the instrument was 10^{-9} Torr. The intensity of the XPS band was determined using linear background subtraction and integration of peak areas. The binding energies were determined by computer fitting the measured spectra and were referenced to the C 1s at 285 eV.

FTIR spectra were obtained using Perkin-Elmer System 2000 equipped with deuterated triglycine sulphate and mercury cadmium telluride detectors. FTIR studies were performed on self-supported wafer (ca. 20 mg) fixed to sample holder of a high temperature FTIR cell fitted with NaCl windows. All samples were first activated under vacuum ($<10^{-4}$ Torr) at 573 K for 16 h. A high purity gases (i) nitric oxide (with 95% nitrogen) and (ii) carbon monoxide

(supplied by Linde, Australia) were used as the NO or CO source. All FTIR spectra were background corrected. The spectra of activated catalyst samples were used as a background from which the adsorbed probe molecule spectra were subtracted. FTIR Spectra were obtained in the mid-infrared region, over the range 4000–1400 cm^{-1}, with 64 co-added scans at 2 cm^{-1} spectral resolutions. The details of instruments utilized and characterization methods are reported elsewhere [12,16,17,21].

3. Results and discussion

The high purity mesoporous (MCM-41 type) and microporous [high silica pentasil zeolite (ZSM-5), low silica faujasite (LSX)] materials containing various loading of gold nanoparticles were prepared. These materials were chosen because they provide high surface area, different micro-or mesoporous structure and could help to contained the gold nanoparticle structure, size and concentration at higher reaction temperatures.

These as-prepared mesoporous and microporous materials were highly crystalline and utilized for the characterization, infrared adsorption and high temperature studies. Au-Al-MCM-41 samples with two different Si/Al and Si/Au ratios and Au-ZSM-5 samples with three different Si/Al and Si/Au ratios were synthesized. The characterization of Au–Al-MCM-41, Au-ZSM-5 and Au-LSX materials by XRD confirmed the high phase purity, structure and crystallinity [20–23]. The chemical analysis of gold nanoparticles containing mesoporous and microporous materials (Table 1) shows that these materials contain different concentration of gold (varying from 0.166 to 2.02 mol%). It is observed from the results that the Si/Au ratios could be easily varied from 47 to 586 in the different (MCM-41, ZSM-5 and LSX) structures as well as the structures can be prepared with similar or different Si/Al ratios. The two mesoporous (Au-Al-MCM-41(a, b) and microporous Au-ZSM-5(c, d)) materials possesses nearly same Si/Al ratios but different Si/Au ratios.

The mesoporous/microporous catalysts prepared with different gold metal loading were used to study the thermal stability, particle size effect, pore containment, surface

Table 1
Chemical composition of gold nanoparticles containing mesoporous and microporous materials

Material type	Product composition (mol%)				
	Au	Al	Si	Si/Au	Si/Al
Au-Al-MCM-41(a)	2.020	2.900	95.080	47.0	32.8
Au-Al-MCM-41(b)	0.386	2.920	96.694	250.0	33.1
Au-ZSM-5(c)	0.166	2.434	97.400	586.0	40.0
Au-ZSM-5(d)	0.990	2.063	96.947	97.9	47.0
Au-ZSM-5(e)	1.161	1.498	97.341	83.8	65.0
Au-LSX(f)	0.646	48.600	50.754	120.6	1.04
MCM-41		2.910	97.090		33.4
ZSM-5		2.160	97.840		45.3

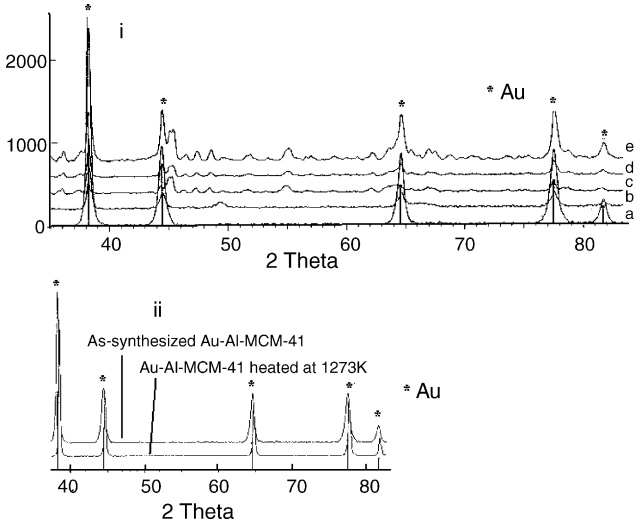

Fig. 1. (i) Powder X-ray diffraction patterns ($2\theta = 35–83^\circ$) of gold nanoparticles in mesoporous and microporous materials. [a) Au-Al-MCM-41(a), b) Au-Al-MCM-41(b), c) Au-ZSM-5(c); d) Au-ZSM-5(d); e) Au-ZSM-5(e).] (ii) XRD patterns ($2\theta = 35–83^\circ$) of the heat treated gold nanoparticles in mesoporous materials at 1273 K [XRD measurements at room temperature].

properties, reactivity towards NO/CO and high temperature structural effects. The XRD patterns of the mesoporous and microporous materials were similar to those of standard MCM-41, ZSM-5 and LSX materials and no changes in their phase were observed. The X-ray diffraction patterns (in the range of $2\theta = 35^\circ–83^\circ$) of the nano-gold particles in the MCM-41, ZSM-5 and LSX structures are shown in Fig. 1(i). The observed XRD peaks (at $2\theta \sim 38.2$, 44.8, 64.8, 78 and 82) are characteristic diffraction lines of Au (1 1 1), Au (2 0 0), Au (2 2 0) and Au (2 2 2) and mostly correspond to FCC metallic gold diffraction. In the XRD patterns, there were no lines related to gold chloride salt crystalline phase indicating the reduction of gold chloride during hydrothermal crystallization process. Fig. 1(ii) shows the XRD pattern of the Au-Al-MCM-41(a) calcined at 1273 K (XRD data collection at room temperature). After heating the as-prepared Au-Al-MCM-41 at 1273 for 5 h, slight shift and changes in the intensities of the peaks were exhibited in the XRD pattern. This shows that gold nanoparticles remains contained in the MCM-41 material even at the high temperature of 1273 K. The particle size and nitrogen sorption data (BET) for Au-Al-MCM-41, Au-ZSM-5 and Au-LSX materials at different calcination temperatures are presented in Table 2. Nitrogen sorption and XRD results indicate that the mesoporous and microporous structure is well maintained after calcination at 773 K. Au-Al-MCM-41 samples possess mostly mesopores as indicated by the pore size distribution from the BET results. The pure Al-MCM-41 and ZSM-5 materials possess higher surface area and micropore volume than the nano gold containing MCM-41 and ZSM-5 materials. The decrease in the higher surface area and micropore volume of these materials is due nano gold particles occupying the certain spaces in the pores of the microporous

Table 2
Particle size and surface characteristics of the gold nanoparticles containing mesoporous and microporous materials

Material type	Gold particle size (nm)	Surface properties of the calcined samples		
		Surface area (m^2/g)	Micropore volume (cm^3/g)	Total pore volume (cm^3/g)
Au-Al-MCM-41(a)[a]	3–6	1272	0.0050	1.350
Au-Al-MCM-41(b)[a]	∼3	933	0.0100	0.935
Au-ZSM-5(c)[a]	∼2–4	475	0.1650	0.185
Au-ZSM-5(d)[a]	2–5	517	0.2000	0.240
Au-ZSM-5(e)[a]	∼2–3	549	0.2200	0.290
Au-LSX(f)[a]	∼3	363	0.1550	0.170
Au-Al-MCM-41(a) (1273 K)	>11	1230	0.0040	1.300
Au-Al-MCM-41(b) (1273 K)	>8	899	0.0095	0.900
Au-ZSM-5(c) (1273 K)	∼3–5	396	0.1200	0.120
Au-ZSM-5(d) (1273 K)	3–6	421	0.1100	0.240
Au-ZSM-5(e) (1273 K)	∼6	445	0.2200	0.290
MCM-41		1315	0.0130	1.400
ZSM-5		575	0.2400	0.310

[a] As-prepared samples.

and mesoporous materials. The high temperature calcination of these gold containing materials at 1273 K resulted into decrease in the surface area and micropore volume by ∼3%.

High-resolution transmission electron micrograph (Fig. 2) of the as-synthesised Au-Al-MCM-41(b) shows the spherical shape of gold nanoparticles. The particle size of gold nanoparticles in the as-prepared meso- and microporous materials varied between 2 and 8 nm. TEM analysis of the high temperature treated samples (1273 K) showed that the particle size of gold nanoparticles in the Au-Al-MCM-41(a) and Au-Al-MCM-41(b) was drastically increased by 81 and 33%, whereas in the Au-ZSM-5(c), Au-ZSM-5(d) and Au-ZSM-5(e), the nano gold particle size increased only by 25–45%, respectively, depending upon the gold concentration in the samples. These TEM results clearly indicate that the particle size of gold is affected by the concentration of gold nanoparticles within the mesoporous and microporous materials and the high temperatures.

XPS measurements have been carried out on all the Au mesoporous and microporous samples. The two as-synthesized Au-Al-MCM-41(a) and Au-ZSM-5(e) samples are given in Fig. 3. The binding energy and surface composition data of the nano gold materials are presented in Tables 3 and 4. The C 1s line position is used as a reference for as-synthesized samples. The binding energy (BE) measured for Al 2p, O 1s and Si 2p in the gold mesoporous and microporous catalysts are similar to that of the tetrahedrally coordinated Al 2p, O 1s and Si 2p in the zeolites and metal aluminophosphates [24,25]. The observed Au 4f binding energies in most of the as-synthesised (MCM-41, ZSM-5, LSX) catalysts corresponds to that of metallic gold as well as Au^+, Au^{3+} species. The observed BE of gold species are slightly different in the mesoporous and microporous catalysts. The XPS spectra corresponding to gold (Fig. 3) shows that there are several gold species on the as-synthesised Au-Al-MCM-41(a) and Au-ZSM-5(e) catalysts. The gold species present on these two catalysts can be classified into metallic gold (Au BE ∼83.5 eV) and ionic gold [Au^{3+} (BE ∼87.0 eV (Au_2O_3) and (90.4–91 eV) $Au(OH)_2^+$)] [26] (Table 3). The analysis of the peak area data of Au and Au^{3+} species indicates that the ratio of Au:Au^{3+} from as-synthesized Au-ZSM-5(e) is

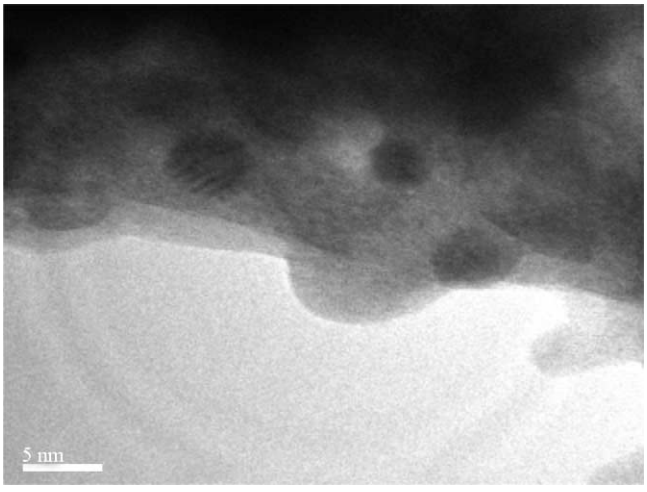

Fig. 2. TEM of as- synthesized Au-mesoporous material.

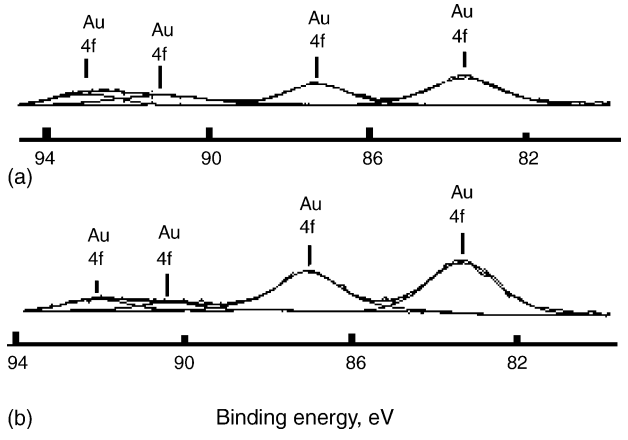

Fig. 3. XPS pattern of gold nanoparticles in mesoporous and microporous materials. (a) Au-Al- MCM-41(a), (b) Au-ZSM-5(e).

Table 3
XPS binding energy data on the gold nanoparticles containing mesoporous and microporous materials

Element	Sample											
	Au-Al-MCM-41(a)[a] (eV)	Au-Al-MCM-41(a)[b] (eV)	Au-Al-MCM-41(a) (1273 K) (eV)	Au-Al-MCM-41(b)[a] (eV)	Au-Al-MCM-41(b)[b] (eV)	Au-ZSM-5(c)[a] (eV)	Au-ZSM-5(c)[b] (eV)	Au-ZSM-5(d)[a] (eV)	Au-ZSM-5(d)[b] (eV)	Au-ZSM-5(e)[a] (eV)	Au-ZSM-5(e)[b] (eV)	Au-LSX(f)[a] (eV)	Au-LSX(f)[b] (eV)
Al 2p	73.0	73.2	73.4	73.0	75.1	73.3	74.3	73.1	73.8	73.5	74.1	73.6	73.8
Au 4f7/2	83.3	84.1	84.3	83.3	84.1	83.4	83.5	83.5	83.7	83.6	83.7	84.0	84.1
Au 4f5/2	87.0	87.8		86.9	87.2	87.0	87.2	87.2	87.2	87.3	87.4	86.8	86.9
Au 4f	90.4									91.3			
Au 4f	92.1									93.1			
N 1s	402.2			402.4		401.7		401.7		401.7			
Na 1s												1072	1072
O 1s	531.8	533.0	532.6	532.2	533.5	532.3	533.2	532.4	533.3	532.5	533.2	531.2	531.3
Si 2p	102.8	103.2	102.9	102.7	103.9	102.9	103.8	102.6	103.8	102.2	103.6	101.7	102.0
K 2p												294.1	293.6

[a] As-prepared materials.
[b] Sample calcined at 773 K.

less than from as-synthesized Au-Al-MCM-41(a). At higher treatment temperature of 1273 K, all the gold species are converted mostly to metallic Au. The slight shift in the binding energies of Au is observed for all the calcined samples.

The results of bulk chemical and XPS surface (Table 4) analysis of the as-synthesized meso- and micro porous catalysts indicated that the Si:Al ratio on the surface is higher than that in bulk. This indicates that the concentration of aluminium is lower on the surface of these materials. In case of the calcined samples, the surface Si/Al ratio decreases indicating that the surface concentration of aluminium increases after the heat treatment. Comparison of the bulk and surface Si:Au ratio in the as-synthesized Au-Al-MCM-41(a), Au-ZSM-5(e) and Au-LSX(f) indicated that the bulk concentration of the gold metal atom is slightly lower than the surface of these materials and gold is homogeneously distributed in the materials. The distribution of gold metal is different on the surface and bulk of the meso- and micro porous materials. However, after calcination of the samples at different temperatures (773 and 1273 K), the concentration of surface gold increases which is indicated by the decrease in surface Si/Au ratio. This decrease is due to migration and clustering of gold atoms at higher temperatures. The changes in the gold particle size are confirmed by the EXAFS and TEM studies (Table 2).

Our previous XAS results [12] showed the presence of few oxidic gold (Au-O) and most of metallic gold species (Au-Au). The similarity of XANES and Fourier transforms in various structures (MCM-41, ZSM-5, LSX) with different gold concentration indicates the local structure around the gold atom is very similar despite of the material structure. In the Au-LSX, the signals observed between 1.2 and 2.0 Å are prominent than the other Au-materials. On the radial distribution curve, the characteristic profile of metallic gold is easily recognized (Au-Au $\sim 2.72 \pm 0.02$ Å). A signal at about 1.6–1.8Å observed in the radial distribution curve is characteristic of oxidized gold surrounded by light atoms (mostly short Au–O bond) [12]

The major troublesome components of exhaust gas produced by the stationary and mobile sources are nitric oxide and other NO_x gases. These components are easily reduces to nitrogen using different platinum metal catalysts. Haruta and Ueda [27] demonstrated the application of gold catalysts for the reduction of NO outperforms the other catalysts under oxygen free environment and at lower temperature with limitation at higher temperatures. Gold supported on various metal (Fe/Zn/Mg/Ti/Al) oxides are active catalysts for the reduction of NO with propylene/O_2/moisture. The highest conversion to nitrogen was obtained over Au/Al_2O_3 with metal loading of 0.1–0.2 wt.% at 700 K [28].

Interaction of NO with nano gold mesoporous and microporous catalysts is depicted in Figs. 4–6. The nature of sites, the oxidation state of the metal and the state and localization of the cations on the catalyst surface are usually investigated using NO adsorption and a FTIR technique. After vacuum dehydration of the nano gold catalysts at 573 K for 16 h,

Table 4
XPS surface composition of the selected gold nanoparticles containing mesoporous and microporous materials

Element	Sample						
	As-prepared Au-Al-MCM-41(a)	Calcined Au-Al-MCM-41(a) (773 K)	Calcined Au-Al-MCM-41(a) (1273 K)	As-prepared Au-ZSM-5(e)	Calcined Au-ZSM-5(e)	As-prepared Au-LSX(f)	Calcined Au-LSX(f)
Al 2p	0.80	0.90	0.94	0.46	0.16	2.47	2.52
Au 4f7	0.30	1.24	1.90	0.13	0.44	0.05	0.10
Au 4f5	0.20	0.82	1.40	0.10			
Au 4f	0.02			0.05			
Au 4f	0.02			0.07			
C 1s	34.30	4.60	6.70	18.50	4.00	1.73	5.85
N 1s	2.10			0.80			
Na 1s						24.38	19.13
O 1s	50.48	81.44	78.86	51.79	81.90	61.15	63.25
Si 2p	11.60	11.00	10.20	28.10	13.50	5.09	4.75
Si/Al	15.13	12.22	10.85	61.08	84.37	2.06	1.88
Si/Au	23.00	5.33	3.09	80.28	30.68	101.80	47.5
Bulk Si/Au	47.00			84.00		120	
Bulk Si/Al	32.8	31.60	30.10	65.00	64.20	1.04	1.05

exposure to NO resulted in more than four/five bands attributed to the formation of nitrous oxide (N_2O), chemisorbed nitrogen dioxide (NO_2), mononitrosyl (M-NO), dinitrosyl [M-$(NO)_2$], and nitrite (M-NO_2) complexes. The infrared bands assignment is consistent with the published literature [29–35]. The reactive O^- site reacts with another NO molecule to produce a M-NO_2 complex with a vibrational band at 1630 cm^{-1}. Nitrosyl species resulting from the reaction between nitric oxide and nano gold catalysts are summarized in Table 5. In case of the Au-Al-MCM-41(a), exposure to 22 Torr NO (Fig. 4(a)) produced four bands attributed to the formation of N_2O (2240 cm^{-1}), Au-NO (1906 cm^{-1}), chemisorbed NO (1690 cm^{-1}) and Au-NO_2 (1630 cm^{-1}). In case of the Au-ZSM-5 (d), exposure to 22 Torr NO (Fig. 5(a)) produced four bands attributed to the formation of chemisorbed NO_2 (2170 cm^{-1}), Au-NO (1900 cm^{-1}), Au-$(NO)_2$ asymmetric (1850 cm^{-1}), Au-$(NO)_2$ symmetric (1745 cm^{-1}) while the Au-LSX(f) (Fig. 6(a)) exhibits infrared bands attributed to the formation of N_2O,

Table 5
Infrared bands of species resulting from the adsorption of NO with the gold nanoparticles containing mesoporous and microporous materials

NO_x species	Wavenumber (cm^{-1})
N_2O	~2240
M-NO	~1910
M-$(NO)_2$ (asymmetric)	~1845
M-$(NO)_2$ (symmetric)	~1745
NO_2 (chemisorbed)	~2170
NO_2 (chemisorbed)	~1690
M-NO_2	~1630
M-NO_3	~1590

M denote active metal sites.

chemisorbed NO_2 (2170 cm^{-1}), Au-NO (1900 cm^{-1}) and Au-NO_2 (1630 cm^{-1}). The Au-Al-MCM-41(a) catalyst (Fig. 4), (containing higher amount of gold) shows different concentration distribution of NO_x species than those over the lower gold containing Au-ZSM-5(d) and Au-LSX(f) (Figs. 5 and 6) catalysts.

NO adsorption experiments at different pressures were carried out in order to study the influence of NO gas

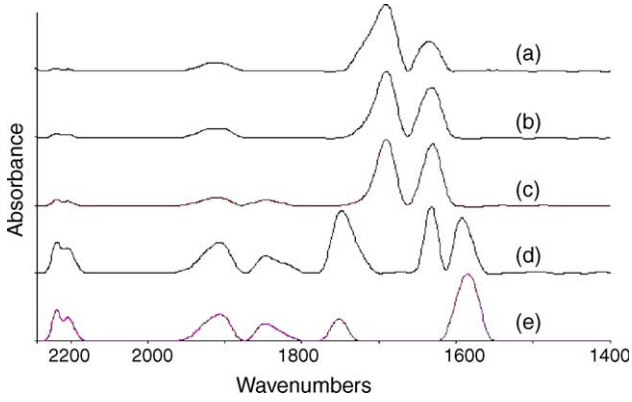

Fig. 4. In situ FTIR spectrum of NO adsorption over the dehydrated Au-Al-MCM-41(a) catalyst: (a) 22 Torr, 298 K, (b) 61 Torr, 298 K, (c) 103 Torr, 298 K, (d) 103 Torr, 423 K, and (e) 103 Torr, 523 K.

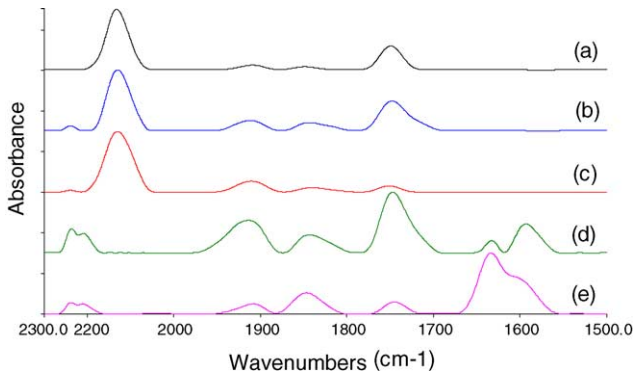

Fig. 5. In situ FTIR spectrum of NO adsorption over the dehydrated Au-ZSM-5(d) catalyst: (a) 22 Torr, 298 K, (b) 61 Torr, 298 K, (c) 103 Torr, 298 K, (d) 103 Torr, 423 K, and (e) 103 Torr, 523 K.

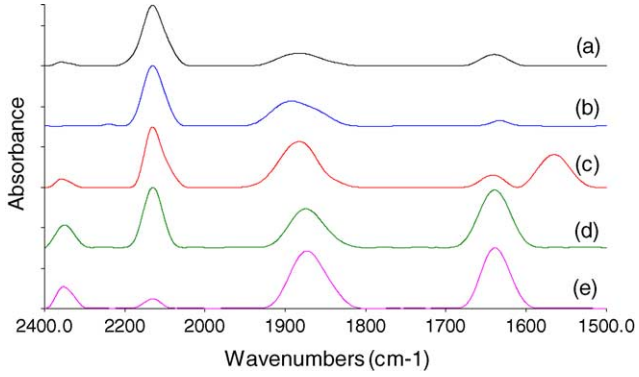

Fig. 6. In situ FTIR spectrum of NO adsorption over the dehydrated LSX(f) catalyst: (a) 22 Torr, 298 K, (b) 61 Torr, 298 K, (c) 103 Torr, 298 K, (d) 103 Torr, 423 K, and (e) 103 Torr, 523 K.

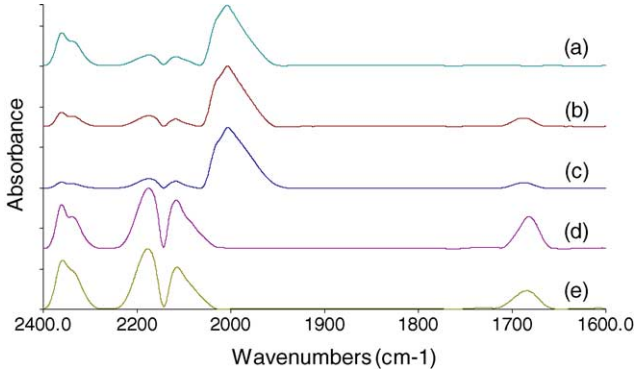

Fig. 7. In situ FTIR spectrum of CO adsorption over the dehydrated Au-Al-MCM-41(a) catalyst: (a) 22 Torr, 298 K, (b) 61 Torr, 298 K, (c) 103 Torr, 298 K, (d) 103 Torr, 423 K, and (e) 103 Torr, 523 K.

pressure on the gold–nitric oxide complexes. FTIR results pertaining to different surface coverage of NO on the Au-Al-MCM-41(a), Au-ZSM-5(d) and Au-LSX(f) (Figs. 4–6(a–c)) shows the changes in NO absorbance at different sites located over the gold catalysts. In the mesoporous catalysts (Au-Al-MCM-41(a)), the concentrations of NO_x species at the respective bands (2224,1900, 1690 and 1630 cm^{-1}) are significantly affected with increasing NO pressure. At highest NO pressure of 103 Torr, an additional band appears at 1850 cm^{-1}, which is related to M-$(NO)_2$ species. NO adsorption studies on the mesoporous catalyst with lower gold content (high Si/Au ratio 250) [Au-Al-MCM-41(b)] exhibited similar NO_x species but with low concentration to that of Au-Al-MCM-41(a). In the microporous Au-ZSM-5(d) catalyst, the increased NO pressure (62, 103 Torr) affects the NO_x species concentrations at the respective bands (2170, 1907, 1850 and 1745 cm^{-1}). At NO pressure of 103 Torr, the concentration of M-NO, M-$(NO)_2$ asymmetric and M-$(NO)_2$ symmetric is decreased. Similar trends were observed for the other Au-ZSM-5 catalysts with different Si/Au ratios. Moreover, in the case of Au-LSX(f), the concentration of Au-NO and Au-NO_2 species on the catalyst surface increased with the incremental dosage of NO. It is interesting to note that the behaviour of gold nano particle is different in mesoporous and microporous system as indicated by the formation of different types NO_x species.

The decomposition of adsorbed NO species at different temperatures and constant pressure over the dehydrated Au-Al-MCM-41(a) Au-ZSM-5(d) and Au-LSX(f) catalysts is shown in Figs. 4–6(c–e). Influence of temperature were investigated at a constant NO pressure (103 Torr) and at 423 and 523 K for 40 min. The NO_x species peak intensities as function of temperature showed interesting trends. By increasing the reaction temperature to 423 and 523 K (Figs. 4–6(d and e)), the chemisorbed NO_2/M-$(NO)_2$ moieties decomposed to mono- and dinitrosyl species. The temperature influences the NOx distribution and decomposition on the Au-ZSM-5 and Au-LSX catalysts. In case of the Au-ZSM-5(e), complete decomposition of the N_2O occurred at 523 K. The changes in ratios of NO_x species indicated strong variation of the surface concentration and distribution of NO complexes with the temperature. Formation of a higher oxidation state species occurs when the dinitrosyl complex is oxidized by NO and forms an unstable complex with N_2O and O^- adsorbed species. Further reaction with NO leads to conversion of the unstable N_2O and O^- intermediates to a nitrite moieties. It is evident from the NO_x results that the reaction-interaction of NO_x species is strongly affected by the gold nanoparticles as well as their location/distribution in the host structures.

CO oxidation has been an area of extensive research, particularly its conversion to carbon dioxide. Haruta [36] have investigated the effectiveness of the gold cluster catalyst in oxidation of CO. Au-based catalysts have extraordinary activity for removal of CO at room temperature and below. CO adsorption technique provides information about the oxidation and coordination state of charge balancing cations and widely employed for analysis of active sites on nano gold materials. Nano gold catalysts were used to investigate the interaction of CO using the in situ FTIR technique. The interaction between CO and Au-Al-MCM-41(a) and Au-ZSM-5(d) is presented in Figs. 7 and 8. After dehydration of Au-Al-MCM-41(a) in vacuo at 573 K for 18 h, exposure to CO (22 Torr) produced vibrational spectra with up to seven infrared bands

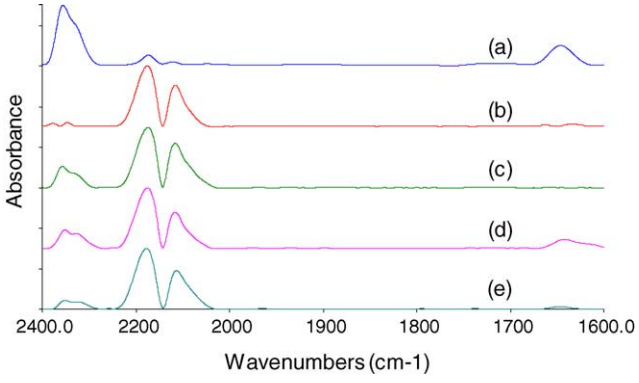

Fig. 8. In situ FTIR spectrum of CO adsorption over the dehydrated Au-ZSM-5(d) catalyst: (a) 22 Torr, 298 K, (b) 61 Torr, 298 K, (c) 103 Torr, 298 K, (d) 103 Torr, 423 K, and (e) 103 Torr, 523 K.

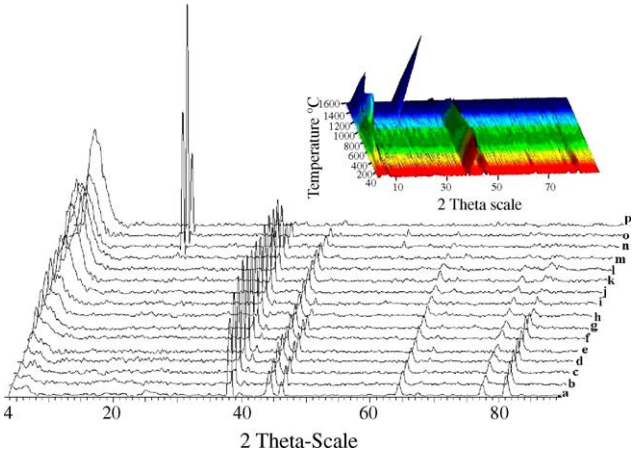

Fig. 9. In situ high temperature XRD analysis of gold nanoparticles in MCM-41 mesoporous materials (a, 413 K; b, 473 K; c, 573 K; d, 673 K; e, 773 K; f, 873 K; g, 973 K; h, 1073 K; I, 1173 K; j, 1273 K; k, 1373 K; l, 1472 K; m, 1573 K; n, 1673 K; o, 1773 K; and p, 1873 K) (*x*-axis shift: 1 mm/XRD pattern).

attributed to the formation of physisorbed carbon dioxide (CO_2) (2350 cm^{-1}), CO chemisorbed on Au^+ (2180 cm^{-1}) and intrazeolite Au^+ (2192 cm^{-1}), CO adsorbed on Au metal (2124 cm^{-1}), bridged metal carbonyl complexes (Au-CO-Au)/ Lewis acid sites (L-CO) (2004, 2024 (shoulder) cm^{-1}). At CO pressure of 22 Torr, the dehydrated Au-ZSM-5(d) exhibited the bands related to physisorbed carbon dioxide (CO_2) (2360 cm^{-1}), CO chemisorbed on Au^+ (2182 cm^{-1}), CO adsorbed on Au metal (2124 cm^{-1}) and encapsulated carbon dioxide (CO_2) (1632 cm^{-1}). The band at 2182 cm^{-1} is interpreted in terms of CO attached to Au^+ species with acidic Al^{3+} and H^+ sites in zeolitic materials [37]. These infrared bands are consistent with the reported literature for microporous materials [16,25,29–35,38–40]. FTIR CO adsorption studies on the other Au-Al-MCM-41(b), and Au-ZSM-5(c) catalysts with higher Si/Au ratios (lower concentration of gold nanoparticles) showed similar type of CO species but with lower concentrations of these species to that of the mesoporous and microporous catalysts with lower Si/Au ratios (higher concentration of gold nanoparticles). This indicates that the type CO species formed are (up to certain extent) unaffected by the concentration of nano gold particles in mesoporous and microporous materials.

CO adsorption on activated gold catalysts [Au-Al-MCM-41(a) and Au-ZSM-5(d)] at 298 K and increasing equilibrium pressures and temperatures is depicted in Figs. 7 and 8(a–e). In case of the Au-Al-MCM-41(a) and Au-ZSM-5(d), the band related to physisorbed CO_2 was significantly affected by increase in the CO pressure. In case of mesoporous Au-Al-MCM-41(a), (above 423 K), a marked increase in intensity of the CO chemisorbed on Au^+, CO adsorbed on Au metal, physisorbed carbon dioxide and decrease in the bridged metal carbonyl complexes (Au-CO-Au)/Lewis acid sites (L-CO) was observed. The dominance of the CO-Au^+ and CO-Au metal bands indicates the stability of these species over the bridged metal carbonyl complexes (Au-CO-Au)/Lewis acid sites (L-CO). Similar trend was observed for the Au-Al-MCM-41(b) and Au-LSX with the different gold concentrations. In the Au-ZSM-5(d), the band related to CO-Au^+ and CO-Au metal bands were unaffected at the high reaction temperatures.

From the NO and CO adsorption studies, it can be seen clearly that apart from nano gold particles, the host support type as well as the constraint imposed by the structure on the interaction of nano gold particle with reactant molecule influences the formation of NO_x and CO species.

The high temperature in situ XRD patterns of gold nanoparticles in mesoporous and microporous structures are shown in Figs. 9 and 10. Gold nanoparticles in various forms are gaining wide spread application in catalysis and other areas. However, the major problem faced with gold nanoparticles is the agglomeration of gold nanoparticles to bigger metallic particles, thus affecting the unique nano gold properties during catalyst processing above 373 K, high temperature catalysis and use in various high temperature applications. The agglomeration/clustering of gold nanoparticles is due to of low sublimation energy/melting point of gold, which results into changes in the particle size and other properties of gold nanoparticles. Apart from the gold properties influencing agglomeration, the type and structure of support play critical role in maintaining the structure of nanoparticles. So far in literature, most of the nanoparticles studies reported were based on using the support materials with low surface area (<100 m^2/g)[5–9,27,28].

The in situ high temperature XRD (HTXRD) measurements was undertaken to investigate the fate of gold nanoparticles and the influence of mesoporous and microporous support structures on the containment of the nanoparticles at different temperatures (313–1873 K). The in situ HTXRD measurements on as-prepared Au-Al-MCM-41(a) and Au-ZSM-5(d) were conducted in vacuum with heating rate of 5 K/min and 1 h as a holding period for each temperature step. In case of the mesoporous Au-Al-MCM-41(a) material (Fig. 9), the in situ HTXRD results showed that no changes in the phases of gold and support were observed up to the temperature of 1573 K. However, above the temperature of 1573 K, the mesoporous support (MCM-41) phase changed to cristobalite phase and further no changes in cristobalite phase was observed up to 1873 K. At high temperature (>1673 K) some minor peaks ($2\theta = 37.8^\circ, 45.5^\circ$) related to Au_3Si and Au_2Si were observed. In case of the microporous Au-ZSM-5(d) material (Fig. 10), the in situ HTXRD results showed that no changes in the phases of gold and ZSM-5 were observed up to the temperature of 1473 K. However, the ZSM-5 phase collapsed above 1573 K to form the cristobalite/tridymite phases. The changes in the concentration of gold particles with the temperature are very interesting over the mesoporous and microporous support structures (Fig. 11). In Fig. 11, the relative changes in the gold peak ($2\theta = 38.3^\circ$) areas with temperature shows that the concentration of gold in mesoporous and microporous

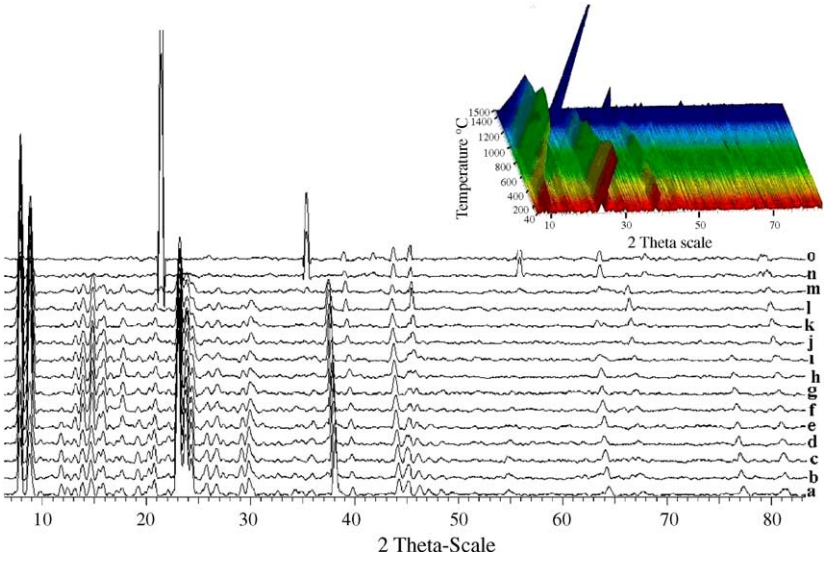

Fig. 10. In situ high temperature XRD analysis of gold nanoparticles in ZSM-5 microporous materials (a, 413 K; b, 473 K; c, 573 K; d, 673 K; e, 773 K; f, 873 K; g, 973 K; h, 1073 K; I, 1173 K; j, 1273 K; k, 1373 K; l, 1472 K; m, 1573 K; n, 1673 K; and o, 1773 K).

material is decreased by increase in the temperature. The significant decline in the gold concentration in both materials starts to occur above the temperature of 1150 K. In case of the Au-Al-MCM-41, at 1473 K approximately 78% of the concentration of gold is contained and 58% of gold is contained at 1573 K. When the temperature is higher than 1573 K, the gold containment is significantly reduced to 27% (∼1673 K), 17% (1773 K) and <5% (1873 K). In case of the Au-ZSM-5(d), approximately 78% of the concentration of gold is contained up to 1223 K and 59% of gold is contained at ∼1373 K while above the temperature of 1473 K, the gold containment is significantly reduced to 19% (at 1573 K), 17% (1773 K) and <2.7% (1673 K). Comparison of these in situ HTXRD results shows that the containment of gold at higher temperatures is higher in the mesoporous Au-Al-MCM-41(a) than in the microporous Au-ZSM-5(d) material.

From in situ HTXRD results, it is observed that substantial amount of gold particles are retained within the mesoporous and microporous materials until the meso- and microstructures are collapsed at high temperatures. This clearly indicate that the gold particle retainment is due to the constrains created by the meso-and microstructures of the materials. These meso- and micro- structures are very important factors for gold particle containment. The removal of gold nanoparticles from the meso- and microporous materials could be envisaged in the following steps: firstly, by high temperature evaporation of gold from external surface of the material and secondly, by the removal of gold particles from internal surfaces (meso- and micro-pores) of these materials because of their structure/pore system collapse at various high temperature stages. The removal of gold particles from external surfaces occurs at lower temperatures then the internal surfaces of these materials, thus contributing to the different amount of gold removal at different temperature stages. It is interesting to note that the gold particles with significant concentration could be effectively contained in the mesoporous and microporous systems at higher temperatures and these systems could be employed in various applications.

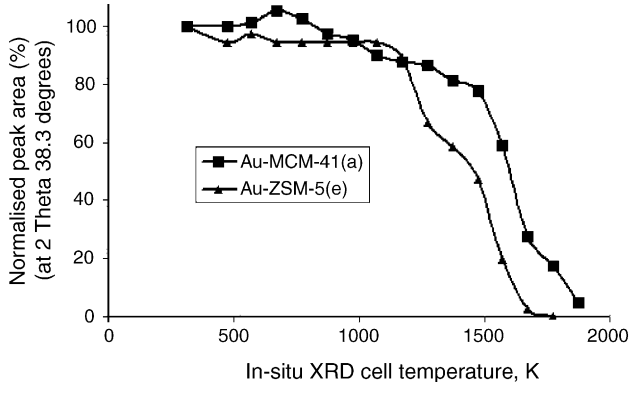

Fig. 11. Relative changes in the gold concentration in the mesoporous and microporous materials with the treatment temperatures.

4. Conclusions

Gold nanoparticles with different size and concentration could be easily prepared in the high surface area mesoporous (MCM-41) and microporous (ZSM-5, X) materials. The XPS and XAS analysis shows the presence of oxidic and metallic gold species and uniform distribution of gold nanoparticles on the external and internal surfaces of these materials. The nano gold particles within the meso- and microporous materials possess higher thermal stability.

Over the Au-Al-MCM-41, Au-ZSM-5 and Au-LSX, NO adsorption at room temperature leads to the formation of different bands attributed to adsorbed nitrous oxide, chemisorbed nitrogen dioxide, nitrite, mononitrosyl and

dinitrosyl complexes. CO adsorption over the Au-Al-MCM-41, Au-ZSM-5 and Au-LSX lead to the formation of physisorbed carbon dioxide and cationic Lewis acid carbonyl moieties as well as transition metal carbonyl complexes (M-CO). The distribution and formation of these NO or CO complexes are influenced by the nano gold particle, concentration, catalyst structure type, reaction temperature and pressure. The type of NO_x species and their concentration are different in the nano gold mesoporous and microporous materials. FTIR results clearly shows that apart from nano gold particles, the microporous (ZSM-5, LSX) and mesoporous (MCM-41) support structures as well as the created environment influences the formation and distribution of NO_x and CO species.

The in situ XRD measurements on these materials shows that the gold nanoparticles are contained up to very high temperatures in the meso- and microporous materials. The gold particles are released from these materials only after their meso-/micro-structural collapse at high temperatures. The results of this study confirm the suitability of gold nanoparticles within meso-/micro porous systems for the high temperature applications.

References

[1] H.-G. Boyen, Th. Herzog, G. Kästle, F. Weigl, P. Ziemann, J.P. Spatz, M. Möller, R. Wahrenberg, M.G. Garnier, P. Oelhafen, Phys. Rev. B (Condens. Matter Mater. Phys.) 65 (2002) 075412.
[2] T. Kobayashi, M. Haruta, S. Tsubota, H. Sano, Sens. Actuators B1 (1990) 222.
[3] V.V. Gorodetskii, W. Drachsel, Appl. Catal. A: Gen. 188 (1999) 267.
[4] V.P. Zhdanov, B. Kasemo, Surf. Sci. Lett. 511 (2002) 23.
[5] M. Haruta, T. Kobayashi, H. Sano, N. Yamada, Chem. Lett. 405 (1987).
[6] M. Haruta, N. Yamada, T. Kobayashi, S. Iijima, J. Catal. 115 (1989) 301.
[7] M. Haruta, Catal. Surv. Jpn. 1 (1997) 61.
[8] M. Haruta, Catal. Today 36 (1997) 153.
[9] N.M. Gupta, A.K. Tripathi, J. Catal. 187 (1999) 343.
[10] C.H. Walker, J.V. St.John, P.W. Neilson, J. Am. Chem. Soc. 123 (2001) 3846.
[11] B.S. Uphade, Y. Yamada, T. Akita, T. Nakamura, M. Haruta, Appl. Catal. A 215 (2001) 137.
[12] D.B. Akolekar, S.K. Bhargava, J. Synchrotron Rad. 11 (3) (2004) 284.
[13] M. Brust, M. Walker, M. Bethell, D. Schiffrin, R. Whyman, J. Chem. Soc. Chem. Commmun. 801 (1994).
[14] J.Y. Jeon, H.Y. Kim, I.S. Woo, Appl. Catal. B: Environ. 44 (4) (2003) 301.
[15] X. Chen, L. Huang, G. Ding, Q. Li., Catal. Lett. 44 (1997) 123.
[16] D.B. Akolekar, S.K. Bhargava, Stud. Surf. Sci. Catal. 105 (1998) 755.
[17] D.B. Akolekar, S.K. Bhargava, K. Foger, J. Chem. Soc. Faraday Trans. 94 (1) (1998) 155.
[18] K.G. Bhattacharyya, A.K. Talukdar, P. Das, S. Sivasanker, J. Mol. Catal. A 197 (2003) 255.
[19] G. Bellussi, G. Perego, A. Carati, U. Gomaro, V. Fatore, Stud. Surf. Sci. Catal. 37 (1998) 37.
[20] R. Ryoo, J.M. Kim, C.H. Ko, C.H. Shin, J. Phys. Chem. 100 (1996) 17718.
[21] D.B. Akolekar, J. Catal. 143 (1993) 227.
[22] D.B. Akolekar, A. Chaffee, R.F. Howe, Zeolites 19 (1997) 359.
[23] C.T. Kresge, M.E. Leonowicz, W.J. Roth, J.C. Vartuli, J.S. Beck, Nature 359 (1992) 710.
[24] D.B. Akolekar, J. Chem. Soc. Faraday Trans. 90 (7) (1994) 1041.
[25] M. Huang, A. Adnot, S. Kaliaguine, J. Catal. 137 (1992) 322.
[26] J.-N. Lin, J.-H. Chen, C.-Y. Hsiao, Y.-M. Kang, B.-Z. Wan, Appl. Catal. B: Environ. 36 (2002) 19.
[27] A. Ueda, M. Haruta, Gold Bull. 32 (1) (1999) 3.
[28] A. Ueda, T. Oshimaand, M. Haruta, Appl. Catal. B: Environ. 12 (1997) 81.
[29] E. Giamello, D. Murphy, G. Magnacca, C. Morterra, Y. Shioya, T. Nomura, M. Anpo, J. Catal. 136 (1992) 510.
[30] G. Spoto, A. Zecchina, S. Bordiga, G. Richiardi, G. Mata, Appl. Catal. B: Environ. 3 (1994) 151.
[31] K. Hadjiivanov, Catal. Rev. Sci. Eng. 42 (2000) 71.
[32] C. Kladis, S.K. Bhargava, K. Foger, D.B. Akolekar, Catal. Today 63 (2000) 297.
[33] C. Kladis, S.K. Bhargava, K. Foger, D.B. Akolekar, J. Mol. Catal. A: Chem. 171 (2001) 243.
[34] D.B. Akolekar, S.K. Bhargava, Appl. Catal. A: Gen. 207 (2001) 355.
[35] A. Zecchina, S. Bordiga, D. Scarano, G. Petrini, G. Leofanti, M. Padovan, C. Otero Arean, J. Chem. Soc. Faraday Trans. 88 (1992) 2959.
[36] M. Haruta, Catal. Today 36 (1997) 153.
[37] H. Huber, D. McIntosh, G.A. Ozin, Inorg. Chem. 16 (1977) 976.
[38] T.M. Salama, T. Shido, R. Ohnishi, M. Ichikawa, J. Phys. Chem. 1000 (1996) 3688.
[39] V.M. Rakic, R.V. Hercigonja, V.T. Dondur, Microporous Mesoporous Mater. 27 (1999) 27.
[40] K.I. Hadjiivanov, L. Dimitrov, Microporous Mesoporous Mater. 27 (1999) 49.